INORGANIC CHEMISTRY FRONTIERS

RESEARCH ARTICLE

View Article Online
View Journal | View Issue

Cite this: *Inorg. Chem. Front.*, 2026, **13**, 3355

Size-dependent electronic structure of titanium-oxo-alkoxides: exploring quantum confinement at the smallest sizes

Thomas J. Barnes, [a] Bin Wang,[b] Eniola Sokalu, [a] Frank De Proft *[b] and Sebastian D. Pike *[a]

The electronic structures of titanium-(oxo-)alkoxides with 1–18 Ti atoms are studied by UV spectroscopy, revealing size effects. These precise molecules act as the smallest titanium–oxygen systems for comparison with bulk and nanoparticulate TiO_2. The results show that at these ultrasmall sizes, with Ti/O cores of less than 1.5 nm, the energy gap is larger than bulk TiO_2 and increases significantly in the smallest compounds. Electrochemical studies supported by DFT calculations show that the greatest changes in electronic structure occur when moving from a complex with a single Ti atom to a dimeric species with two Ti sites. Constructive interaction of d-orbitals, combined with changes in coordination geometry, result in significantly different Ti-based LUMO energies in monomers, dimers and larger clusters, whilst the O-based HOMO energy level remains similar throughout. Size appears to be the dominating factor for LUMO position and energy gap despite the different connectivities, shapes and surface chemistries in these molecular clusters, which differ from bulk TiO_2. These results link materials chemistry with small inorganic molecules and show that (quantum) size effects remain applicable to the smallest systems. This understanding is important for the rational design of semiconductor materials with optimised properties.

Received 2nd December 2025,
Accepted 15th February 2026

DOI: 10.1039/d5qi02443a

rsc.li/frontiers-inorganic

Introduction

Semiconducting metal oxides, such as titanium dioxide (TiO_2), are important photoactive functional materials used in photocatalytic processes, including as self-cleaning or antibacterial surfaces.[1–5] Thin films of TiO_2 are also important as protective layers and electron transport layers in electronic devices.[6,7] The electronic structure of bulk TiO_2 comprises of a filled (O 2p-based) valence band and an empty (Ti 3d(t_{2g})-based) conduction band. The electronic structure of metal oxides becomes modified as particle sizes become very small due to the quantum confinement effect. At small sizes the electronic structure, built from overlap of the constituent atomic orbitals, ceases to be a continuum of energy states, and discrete energy levels are instead found. As the radius of a crystalline particle drops below that of the material's exciton Bohr radius the valence and conduction bands become narrower resulting in an increase in the 'band gap'. Ultimately, on reaching molecular sizes these discrete energy levels represent the various molecular orbitals delocalised over the structure.

Quantum confinement is best known in quantum dot materials, such as CdSe nanoparticles, which exhibit size-dependent luminescence wavelengths, and the importance of this effect is recognised by the 2023 Nobel Prize in Chemistry for Bawendi, Brus and Ekimov.[8–10] TiO_2 has a wide band gap; reported as 3.00–3.03 (*3.20*) eV for rutile and 3.15–3.20 (*3.42*) eV for anatase, by measurement of the indirect (*or direct*) optical gap[11,12] (note that exact values may vary depending on experimental measurement method),[12] and a small exciton Bohr radius, estimated to be ~0.8 nm for anatase.[13] Quantum size effects in TiO_2 are only predicted for particle sizes with diameters <2 nm (Fig. 1a).[14–17] Even the band gaps of ultrasmall (1.5 nm–3 nm) anatase nanoparticles were shown to have negligible deviation from bulk values.[13,18] In contrast, 3.6 nm rutile nanoparticles have been reported to show a small blue shift compared to the bulk energy gap (*3.38* eV *vs.* *3.2* eV, *by direct transition*).[11] Extended $(NH_4/H)_{4x}Ti_{(1-x)}O_2$ nanosheets (0.7 nm thick) are also reported to have energy gaps of ~3.8 eV,[19] whilst nanofilaments (0.6 × 1.0 nm cross section) have even higher energy gaps of ~4.0 eV (indirect transition).[20] The band gap of sub-monolayer TiO_x deposited on silica is shown to increase with decreasing coverage, as smaller TiO_x species become dominant.[5] Ultrasmall TiO_2 particles produced using dendrimer templates, are reported to show size dependent band gaps ranging from 3.35–3.79 eV as the particle

[a]*Department of Chemistry, University of Warwick, Coventry, UK. E-mail: sebastian.pike@warwick.ac.uk*
[b]*Research Group of General Chemistry (ALGC), Vrije Universiteit Brussel (VUB), Pleinlaan 2, B-1050 Brussels, Belgium*

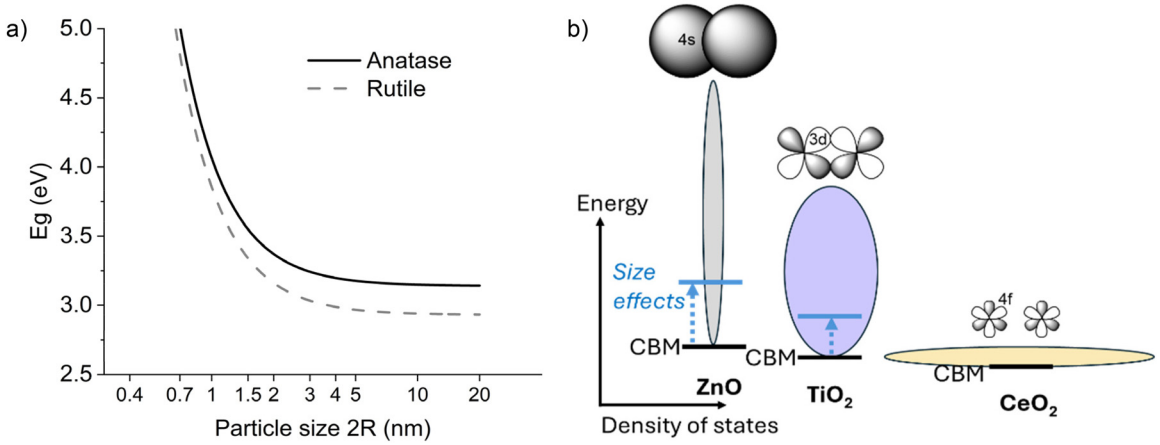

Fig. 1 (a) Band gap prediction for TiO_2 particles based on quantum confinement effects using the effective mass approximation (EMA). Values from the Nosaka equation (similar to Brus equation), with a μ' value of $1.63m_0$.[14] Note that a single TiO_6 octahedron has a size of ~0.4 nm. N.B. the EMA is considered to overestimate energy gap at very small sizes. (b) Depiction of the density of states of the conduction bands of wide band gap oxide semiconductors that are constructed from different types of orbitals, and the response of the CBM with quantum confinement effects.

diameter decreased from 1.7 nm to around 1 nm in size.[14] It is important to note that at these sizes (<100 Ti atoms), the species may be better described as a molecule, in which the surface plays a significant role. Structural distortion may occur due to the tiny size and influence of (bridging) surface ligands. This distortion may lead to changes in coordination geometry, covalency and/or Ti···Ti distances that may compete with intrinsic size effects.

In the related semiconductor ZnO, studies of quantum size effects reveal that the main change in electronic structure is an elevation of the conduction band minimum (CBM), with the valence band maximum (VBM) less effected. In ZnO the conduction band is constructed from diffuse 4s orbitals with good overlap and is, therefore, a wide band, highly susceptible to quantum size effects (Fig. 1b).[21–23] In contrast, in CeO_2, the contracted 4f orbitals are the frontier unoccupied electronic states, and these create a narrow set of energy states which are barely effected by size effects.[24] The 3d orbitals of TiO_2 sit between these extremes,[25] and therefore, some change in CBM position is expected for TiO_2, but only at very small particles sizes.

Molecular chemistry reveals that at <2 nm Ti/O structures adopt different shapes and Ti–O coordination arrangements, showing structural distortion relative to bulk TiO_2 structures. Molecular titanium-oxo clusters, which have a surface stabilised by organic ligands, fall in this size range, and many have been reported with Ti/O cores ranging from 0.5–1.5 nm in size.[17,26–28] However, in these cluster molecules the repeating structure found in rutile or anatase is not typically observed, as at these very small sizes the surface environment dictates coordination geometries and overall structure. Despite changes in structure, <1 nm Ti-oxo clusters are capable of photoexcited charge separation under UV light, and can perform photocatalysis.[29–32] These clusters are closely related to the secondary building blocks in (photoactive) titanium-based MOFs.[33–37] This report investigates to what extent the quantum confinement effect can be extended to understand and predict the electronic structures of a range of Ti-(oxo-)alkoxides with Ti/O core sizes from 0.3–1.3 nm, even if the Ti–O connectivity differs from the parent structure.[38]

Titanium tetra-alkoxides (*e.g.* $[\{Ti(O^iPr)_4\}_n]$) are commonly used precursors for a wide range of compounds and materials, including the formation of TiO_2. Bulky titanium alkoxides such as $[Ti(OAd)_4]$ (Ad = 1-adamantoxide) (Fig. 2) are mononuclear tetrahedral complexes in the solid-state, as confirmed by X-ray crystallography.[39–41] Less bulky alkoxides may crystallise as dimers (neopentoxide, ONp) or tetramers (ethoxide, methoxide), with five or six coordinate Ti centres respectively.[42,43] However, in solution lower degrees of oligomerisation are expected, with the monomeric form dominant for titanium tetra-neopentoxide, isopropoxide and *tert*-butoxide, and the trimeric form dominant for titanium ethoxide (Table S1).[42,44] The partial hydrolysis of titanium-alkoxides to form titanium-oxo-alkoxide clusters was extensively studied by Mosset, Klemperer, Day and Sanchez during the 1990s. Changing the degree of hydrolysis, temperature and reaction pressure can generate Ti-oxo-alkoxides of different sizes, which can be isolated by crystallisation (Fig. 2).[45–51] It is important to note that the smallest clusters such as $[Ti_3O(O^iPr)_9(OMe)]$ (**Ti_3**) form an equilibrium with higher nuclearity clusters and $[Ti(O^iPr)_4]$ when in solution.[45]

A host of different structures, including a large Ti_{52} cluster, can also be prepared by introducing extra organic ligands such as carboxylates or sulphates.[17,26,27,52] These additional ligands may have a significant influence upon electronic structure and can be used for 'band gap engineering', significant changes are noted for cases in which a dye ligand inserts energy levels within the Ti/O based HOMO–LUMO gap.[53,54] Therefore, the simple set of Ti-oxo-alkoxides, without extra surface ligands, are of particular interest for a systematic study of energy gaps *versus* size/nucleation.

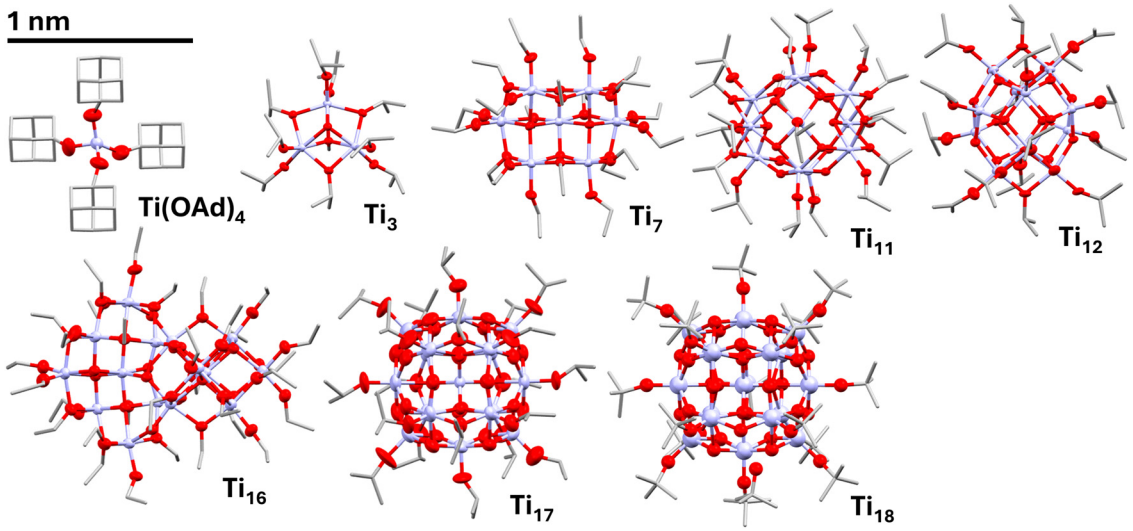

Fig. 2 Crystal structures of $[Ti(OAd)_4]$ and Ti-oxo-alkoxide clusters displayed to scale. Ellipsoids at 50% probability, C atoms displayed as capped sticks and hydrogen atoms omitted for clarity. Ti = lilac, O = red, C = grey.

The energy gaps of some Ti-oxo-alkoxide clusters have been previously reported using UV/visible spectroscopy to determine absorption onset, for example, $[Ti_{17}O_{24}(O^iPr)_{20}]$ (**Ti_{17}**) has a Ti/O spherical core diameter of 1.2 nm and a HOMO–LUMO gap reported as 3.36 (*4.26*) eV using Tauc's method to analyse the solution UV spectrum (in CH_2Cl_2) with a forbidden indirect transition (exponent n = 3, [Ti] = 9 mM) (*or allowed direct transition (exponent n = 1/2, [Ti] = 0.04 mM) respectively*),[55] however, a different value of 3.8 eV was reported using linear extrapolation of the absorption edge from diffuse reflectance UV spectroscopy (DRS) of a powder.[56,57] Both methods indicate a blue-shift of the energy gap from that of bulk TiO_2.

It can be challenging to make direct comparisons between studies due to the different spectroscopic methodologies and analyses conducted across different studies (SI note 1).[58] In this paper we compare the absorption spectra of a range of differently sized Ti-(oxo-)alkoxides using consistent experimental techniques, to qualitatively show size-related absorption shifts.

Results & discussion

Electronic absorption spectroscopy

Solution phase UV spectroscopy was conducted on Ti-alkoxides and Ti-oxo-alkoxides at (consistent) high concentrations ([Ti] = 35 mM) in pentane solvent to most accurately determine changes in indirect absorption onset. Solid-state DRS spectra were also collected for comparison.

To benchmark our data against the literature, the solid-state UV spectrum of bulk anatase and rutile was collected, Tauc's analysis was conducted using n = 2 (*or* $\frac{1}{2}$) for indirect (*and direct*) transitions (*note direct values are given in italics throughout the discussion*). In our hands, the band gap is calculated as 3.1 (*3.3*) eV for anatase and 2.9 (*3.1*) eV for rutile (Fig. 3c, S2). The absorption spectrum of **Ti_{17}** was collected in solution (in duplicate) and in the solid-state and analysed by Tauc's method. To compare with different methodologies of determining absorption onset methods to estimate indirect and *direct* transitions were both used (see experimental methods). Indirect absorption of solution data ([Ti] = 35 mM, exponent n = 3)[55] gave an onset value of 3.6 ± 0.1 eV (literature 3.4 eV),[55] whilst DRS data gave a lower value of ~3.2 eV. The *direct* absorption value from low concentration solution data ([Ti] = 0.11 mM, exponent n = 1/2) was *4.3 ± 0.1 eV* (literature *4.3 eV*)[55] but from solid-state data gave *3.5 ± 0.1 eV*. The difference between solution and solid-state data is greater than observed for some other Ti-oxo clusters, *e.g.* only a minor red-shift (<0.1 eV) was previously determined by our research team when comparing solid-state and concentrated solution data, for $[Ti_4O_4(O^iPr)_4(O_2PPh_2)_6]$.[31] However differences between the solid-state and solution spectra of other metal alkoxide species have been previously reported,[24] and perhaps represents the ability of these structures to adjust to surrounding environment. To ensure that the red-shift in the solid spectrum was not due to trace hydrolysis under air, the measurement was repeated in a quartz cuvette sealed within the glovebox with vacuum grease, and this gave a very similar spectrum (which did not change over several days). Comparison of absorption onset values is difficult due to the different ways of calculating them, and differences between solution and solid-state data (Fig. S2), noting the linear absorption scale for solution data, but closer to logarithmic scale for diffuse reflectance data (which emphasizes low intensity features). Therefore, best comparisons are made by collecting absorption spectra under consistent conditions and comparing the spectra themselves.

Titanium alkoxides $[\{Ti(OR)_4\}_n]$ with differing structures (*e.g.* monomers, trimers, tetramers, Table S1, Fig. S3–S6)[44,59] were examined to consider the smallest possible Ti/O systems.

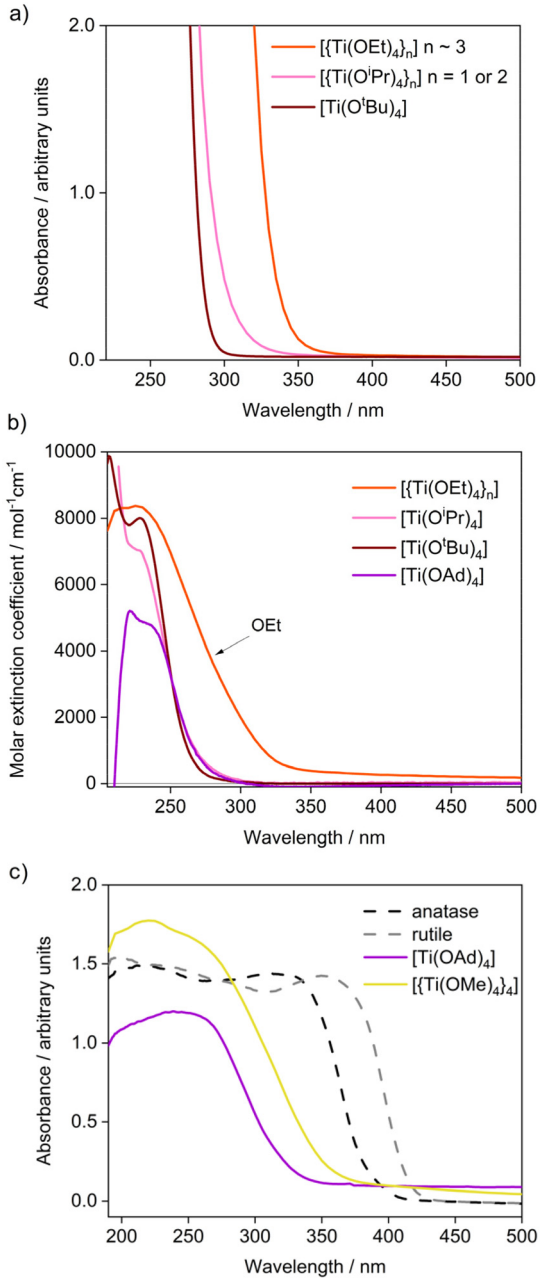

Fig. 3 Solution (a, 35 mM; b, 0.11 mM) and solid-state DRS (c) absorption spectra of titanium tetra-alkoxides.

^{1}H DOSY NMR spectroscopy was used to investigate the degree of oligomerisation in the soluble compounds in d^8-toluene (Fig. S7–S9). Both [Ti(O^{t}Bu)$_4$] (29 mM) and [Ti(O^{i}Pr)$_4$] (35 mM or 1.8 mM) diffuse at similar rates to the solvent, indicating small monomeric molecules dominate with predicted hydrodynamic diameters of 0.67 nm and 0.60 nm respectively (comparable to ~0.75 nm estimated from crystal structure of [Ti(OAd)$_4$]).[42,59] In contrast, samples of [{Ti(OEt)$_4$}$_n$] ([Ti] = 35 mM) diffuse more slowly through solution with an estimated diameter of 0.93 nm (N.B. the trimer is expected to be dominant at this concentration, with an expected diameter of ~0.9 nm).[43,44] Despite the similar aliphatic groups on these titanium alkoxides (R = Et, ^{i}Pr, ^{t}Bu, Ad), significant changes are observed in the absorption spectra, which track with the degree of oligomerisation (Fig. 3). Upon oligomerisation, an increasing number of Ti and O atoms contribute to the electronic structure of the molecule, and, the coordination geometry at Ti also changes from tetrahedral, to trigonal bipyramidal (on dimerization) and then to octahedral in larger oligomers. Monomeric [Ti(OAd)$_4$] and [Ti(O^{t}Bu)$_4$] absorb only from deep in the UV at 4.3 (*4.8*) and 4.2 (*4.9*) eV (Fig. 3a and b, S10–S13, [Ti] = 35–1.75 mM (*0.1 mM*)). The initial absorbance maxima for [Ti(O^{t}Bu)$_4$] at 228 nm is consistent with studies of isolated tetrahedrally coordinated Ti sites in mesoporous silica.[60,61] A 35 mM solution of [{Ti(O^{i}Pr)$_4$}$_n$], which may contain dimers, absorbs from slightly lower energy of 4.0 eV, however, reducing the concentration to within the range at which monomers are expected to dominate (1.75–0.11 mM) gives values of 4.3 *(4.9) eV* consistent with the other monomers (Fig. 3a and b, S14 and S15). [Ti(OEt)$_4$]$_n$, which is expected to be mainly trimeric in solution,[44,59] absorbs from 3.6 eV (Fig. 3a and b, S16 and S17, [Ti] = 35 mM), with a significantly lower onset energy than the other alkoxides at the same [Ti] concentration (Table S2, N.B. identical spectra are also recorded in THF or EtOH solution).

Monomeric [Ti(OAd)$_4$] and tetrameric [{Ti(OMe)$_4$}$_4$] were also studied in the solid-state by DRS (Fig. 3c, S18–S20). The absorption onset of tetrameric [{Ti(OMe)$_4$}$_4$], at 3.4 (*3.8*) eV, is red shifted relative to [Ti(OAd)$_4$] which absorbs from 3.6 (*4.1*) eV consistent with the degree of oligomerisation in the structure. It is again worth noting the difference between solid-state and solution methods for [Ti(OAd)$_4$]. This compound is highly air sensitive and, even in a vacuum grease sealed quartz cell, the spectrum of [Ti(OAd)$_4$] develops a shoulder over time (after three days the onset becomes shifted to 3.5 (*3.7*), Fig. S20), indicating some hydrolysis of the structure and formation of extended multinuclear species.

Immediate red-shifts in the absorption onset of [Ti(O^{i}Pr)$_4$] are observed in solution upon adding trace water or exposing to air, as species such as [Ti$_3$O(O^{i}Pr)$_{10}$] are generated (Fig. S21).[45] Ti-oxo-alkoxides ([Ti$_3$O(O^{i}Pr)$_9$(OMe)], (**Ti$_3$**);[45] [Ti$_7$O$_4$(OEt)$_{20}$], (**Ti$_7$**);[62] [Ti$_{11}$O$_{13}$(O^{i}Pr)$_{18}$], (**Ti$_{11}$**);[48] [Ti$_{12}$O$_{16}$(O^{i}Pr)$_{16}$], (**Ti$_{12}$**);[48] [Ti$_{16}$O$_{16}$(OEt)$_{32}$], (**Ti$_{16}$**);[50] **Ti$_{17}$**,[49] [Ti$_{18}$O$_{28}$H(O^{t}Bu)$_{17}$], (**Ti$_{18}$**),[51] see Table S3 for sizes) were prepared as crystalline solids by hydrolysis and condensation reactions, and purity was confirmed by solution ^{1}H NMR spectroscopy (Fig. S22–S26). Note that as **Ti$_3$** is susceptible to forming equilibria in solution, the structure was confirmed by single crystal X-ray diffraction, and the most reliable absorption spectrum was measured in the solid state. The solution spectra for all other compounds (Fig. 4, S27–S50), dissolved in pentane, display Beer–Lambert behaviour across a wide concentration range.[45]

Ti$_3$ shows an onset of 3.5 (*3.6*) eV in the solid-state, similar to that of similarly sized [{Ti(OMe)$_4$}$_4$] (Fig. 4c, S27 and S28), and an approximate value of 3.7 (*4.5*) eV in solution (noting possible equilibria) which is similar to trimeric [Ti(OEt)$_4$]$_n$ (Fig. S29). The absorption onsets of the larger Ti-oxo-alkoxide

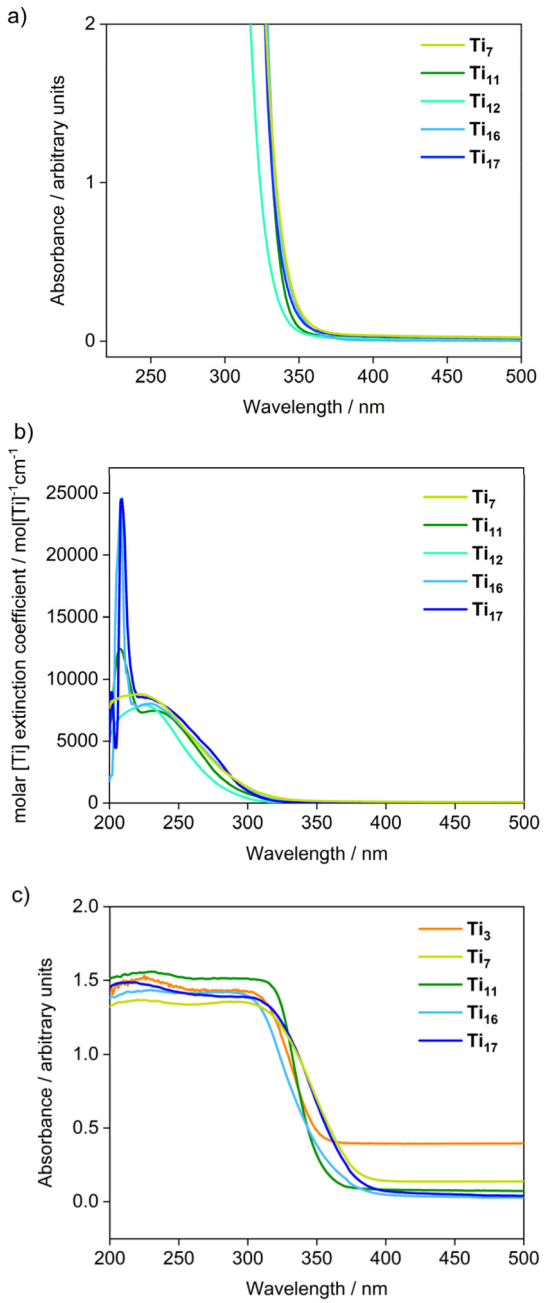

Fig. 4 Solution (a) [Ti] = 35 mM; (b) [Ti] = 0.11 mM (for [Ti] = 1.75 mM see Fig. S50) and (c) solid-state DRS absorption spectra of titanium-oxo-alkoxides.

clusters have similar onsets to each other (Table S2), with minor shifts that do not correlate with nuclearity (**Ti$_7$**, **Ti$_{11}$**, **Ti$_{12}$**, **Ti$_{16}$**, **Ti$_{17}$**: solution (indirect) data range, 3.5–3.6 eV; solid state (*direct*) data range, *3.4–3.6 eV*). Across this size range (maximum core dimension 0.9–1.3 nm, Table S3) small increases in nuclearity have a minor effect, and other factors such as coordination geometry and structural distortion may be influential in determining their exact absorption onsets, masking any size effects (N.B. due to differing shapes **Ti$_{16}$** has a larger maximum dimension than **Ti$_{18}$**). All clusters do remain blue-shifted relative to bulk TiO_2 hinting that to reach bulk values, further order-of-magnitude increases in nuclearity are required.[13] When compared to the effective mass approximation prediction (Fig. 1a, S51), the data collected in this study shows a slower change in energy gap with decreasing size. Of course, the structures at this size no longer resemble bulk anatase or rutile and, therefore, the theoretical model (designed for larger nanomaterials with consistent structure and properties) becomes less valid.

It is noteworthy that after partial hydrolysis, these larger Ti-oxo-alkoxide clusters are more stable to onward hydrolysis than the previously discussed Ti-alkoxides. The powder X-ray diffraction pattern of microcrystalline **Ti$_{16}$** was collected after various times under air, and these results show that crystallinity is retained for over 24 hours but is lost after 1 week (Fig. S52).

Electrochemistry

Cyclic voltammetry measurements were performed on monomeric $[Ti(O^tBu)_4]$, oligomeric $[\{Ti(OEt)_4\}_n]$ ($n \sim 3$) and larger **Ti$_{16}$** and **Ti$_{17}$** to estimate reduction potential and, therefore, LUMO energy (which corresponds to CBM in a molecular species). Electrochemistry was performed inside a glovebox, using a boron-doped diamond working electrode,[63] dry supporting electrolyte (0.1 M $[^tBu_4N][PF_6]$ in dichloromethane; 5–6 ppm water), and 100 mV s^{-1} scan rate in order to successfully observe peaks at significantly reducing voltages. All species show irreversible redox processes and, therefore, Ep_cathodic (maximum peak current of the reductive peak) is extracted as an approximation for redox potential.[64] The data clearly shows a significant shift in reduction potential to more negative energies with decreasing size. **Ti$_{16}$** and **Ti$_{17}$**, with 1.2 nm cores, give similar values of −1.72 and −1.71 V *vs.* Fc/Fc^+. These can be compared to the flatband position of rutile in MeCN (10 ppm water), reported at −1.54 *vs.* Fc/Fc^+, noting that, in this study, the CBM is estimated ~0.01–0.1 eV more negative than the flatband value.[65] This positions the LUMO of 1.2 nm Ti-oxo clusters slightly more negative than Rutile (which is, in turn, generally considered more negative than Anatase by ~0.16 eV).[65] $[\{Ti(OEt)_4\}_n]$ gives a value of −1.92 V, requiring a more reducing voltage to accept an electron, whilst the smallest species $[Ti(O^tBu)_4]$ requires a remarkable −2.56 V to become reduced. The changes in reduction potential (steps of 0.2 & 0.64 V for the sequence **Ti$_{16}$**, $[\{Ti(OEt)_4\}_n]$, $[Ti(O^tBu)_4]$), are similar to the changes in solution absorption onset (steps of 0.03 & 0.61 eV), which suggests that the major changes in electronic structure are due to a changing LUMO position, and that, if at all, the HOMO may be shifted to slightly more negative values, likely due to different oxygen environments in the smallest species (Fig. 5b). To explore frontier orbital energies further, some ethoxide ligands on **Ti$_{16}$** were exchanged with phenoxide. The high lying π orbitals of the phenoxide ligands provide an approximately 'pinned' HOMO level, allowing for analysis of the LUMO energy in this system by the energy gap derived from absorption spectroscopy. The findings, discussed

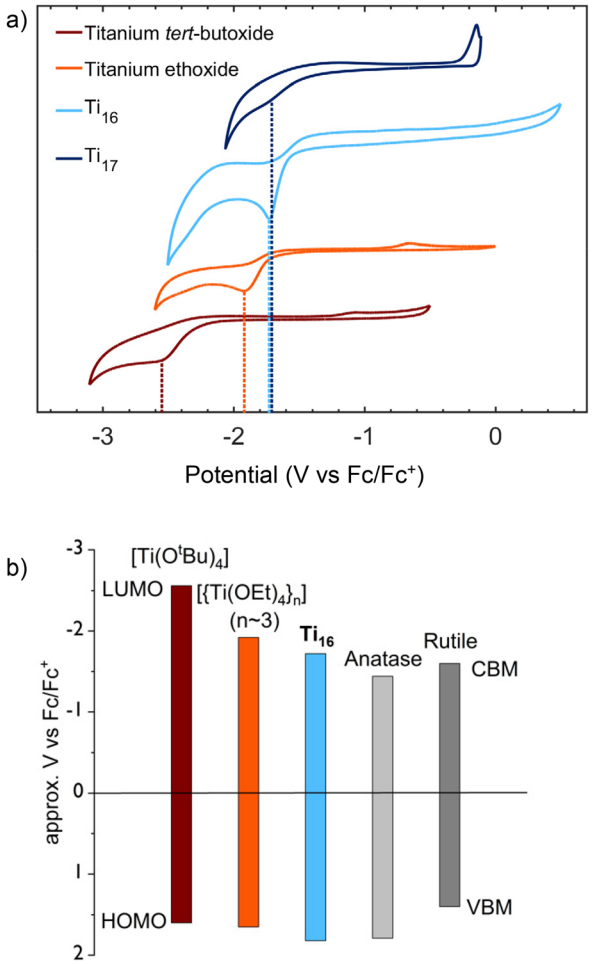

Fig. 5 (a) Cyclic voltammograms of Ti(-oxo)-alkoxides. (b) Approximate energy position of the HOMO–LUMO gap/band gap for selected Ti(-oxo)-alkoxides and TiO_2 polymorphs *vs.* Fc/Fc^+. The LUMO of Ti(-oxo-)alkoxides is approximated at the recorded E_p_cathodic values. Anatase and Rutile frontier energies taken from Kavan *et al.*, estimating CBM at −0.06 eV more negative than flatband energy.[65]

in SI note 2, give a similar result to the electrochemistry studies.

Computational studies

DFT calculations were conducted using Gaussian 16 version A03 on $[Ti(O^iPr)_4]$ (monomer), $[\{Ti(O^iPr)_4\}_2]$ (dimeric form with two bridging O^iPr groups and trigonal bipyramidal coordination geometry at Ti), **Ti$_3$**, $[\{Ti(OMe)_4\}_4]$, **Ti$_7$**, **Ti$_{11}$**, **Ti$_{12}$**, **Ti$_{16}$** and **Ti$_{17}$**.[66–69] Density functional approximations (PBE, TPSSh, PBE0, CAM-B3LYP) with different percentage of Hartree–Fock exchange were employed to scrutinize the magnitude of the band gap. The geometry optimizations were performed using the Def2SVP basis set and the associated single point calculations are performed based on the optimized structure under Def2TZVP basis set for organic atoms with Stuttgart-Dresden effective core potential SDD for the titanium atoms.[70,71] A benchmark study of different functionals for computing the HOMO–LUMO gap is presented in Table S4. Four commonly used density functional approximations (DFAs) for both organic and inorganic systems, PBE, TPSSh, PBE0, and CAM-B3LYP, were applied.[72] Because the Ti cluster is composed of multiple transition metal atoms, the static correlation effect is significant. As shown in Table S4, hybrid and range-separated DFAs overestimate the HOMO–LUMO gap, whereas the pure functional PBE shows the best agreement with the experimental data. Consequently, in the following discussion, only results obtained using the PBE method are presented. However, we expect the trends for different cluster sizes to remain the same with other density functional approximations. The calculations (Table S5) indicate that the LUMO position is the most affected by nuclearity (−1.31 eV change from smallest to largest), with the HOMO remaining similar throughout (all within a 0.39 eV range), consistent with the experimental results (Fig. 6).

The DFT calculations reveal the most significant differences in the electronic structures occur in the smallest systems, caused by changing coordination geometry at Ti (tetrahedral to trigonal bipyramidal to octahedral on increasing nuclearity from one to three) and/or significant mixing of the additional atomic orbitals upon oligomerisation. Monomeric $[Ti(O^iPr)_4]$ shows the expected (e + t_2) LUMO energy levels for d orbitals in a tetrahedral geometry (Fig. S53), while the HOMO is constructed from the 2p orbitals of four interacting O atoms. Overlap of the 3d orbitals on the two Ti centres in the dimeric form, $[\{Ti(O^iPr)_4\}_2]$, creates bonding and antibonding energy d-levels, generating a lower lying LUMO state (0.5 eV more stable than in the monomer). The O based HOMO (already built from a combination of O atomic orbitals) is destabilised by a smaller value of 0.2 eV during dimerization. On extending to **Ti$_3$**, now with an oxo ligand, the LUMO is further stabilised by enhanced 3d interactions (−0.13 eV), but with a signifi-

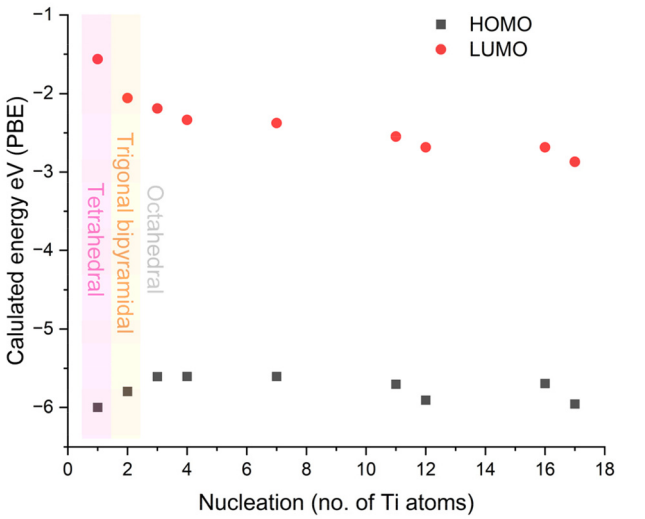

Fig. 6 Calculated HOMO and LUMO energy positions for Ti(-oxo)-alkoxides. The (maximum) coordination number of the Ti atoms is highlighted, note that in larger clusters mixtures of coordination geometries are possible.

cantly smaller jump than from monomer to dimer. The HOMO is also raised by +0.19 eV, with the influence of the oxo ligand observed in the HOMO−1 orbital (Fig. S53). Beyond this size the HOMO remains similarly positioned, with slight deviations across the series, whilst the LUMO steadily drops, with the LUMO of $\mathbf{Ti_{17}}$ stabilised by 0.7 eV compared to $\mathbf{Ti_3}$, presumably due to increasing mixing of d-orbitals with size.

The HOMO and LUMO orbitals of the largest clusters $\mathbf{Ti_{16}}$ and $\mathbf{Ti_{17}}$ are shown in Fig. 7 and S54, in these cases the HOMO is predominantly located on surface oxygens (noting that most oxygens are surface in these small structures). This is consistent with the concept that low coordinate or strained O sites contribute to the highest energy filled electronic states.[24,73,74] The LUMOs are located on Ti 3d orbitals; for $\mathbf{Ti_{16}}$ all Ti are six-coordinate, but the LUMO is mainly located on the most enclosed (core like) sites surrounded by oxo ligands, with much smaller contributions from titaniums with multiple connections to surface alkoxides. In $\mathbf{Ti_{17}}$, six-coordinate Ti sites dominate the LUMO with no contribution from the five and four coordinate sites. Interestingly the central TiO_4 unit in the centre of $\mathbf{Ti_{17}}$ does not strongly contribute to HOMO or LUMO.

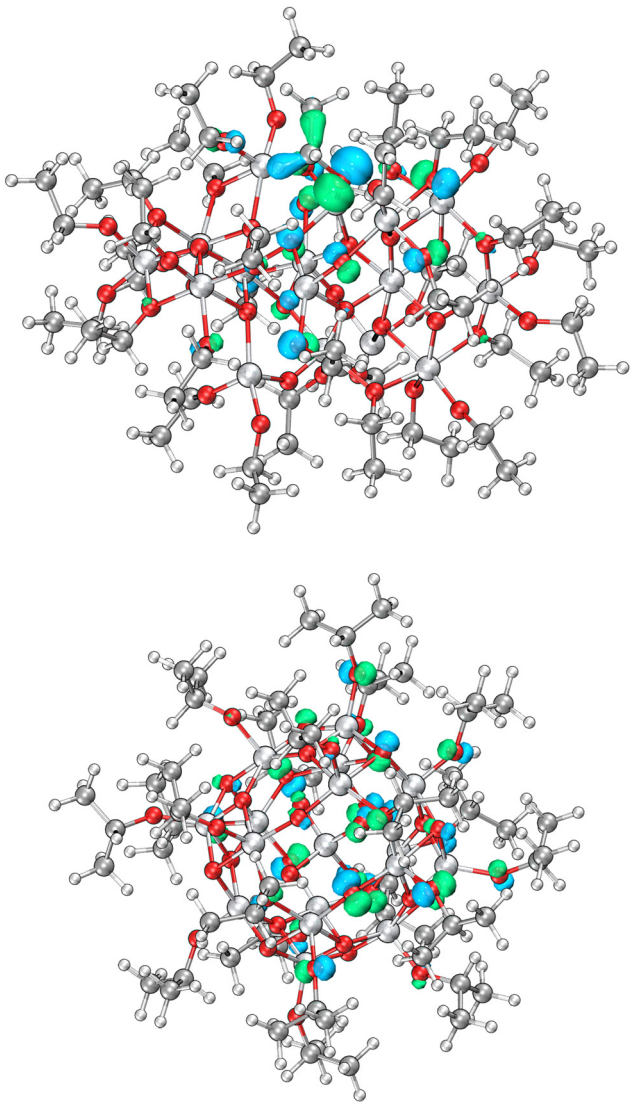

Fig. 7 Calculated HOMO orbitals for $\mathbf{Ti_{16}}$ (top) and $\mathbf{Ti_{17}}$ (bottom).

Conclusions

Electronic size effects are explored in the smallest Ti/O based systems ranging from a single Ti atom to Ti-oxo-alkoxide clusters with ~1.2 nm Ti/O cores. The predominant trend clearly shows that the energy gaps in these systems is related to their size, with energy gap increasing at smallest sizes mostly due to an increase in (Ti-based) LUMO energy. Stabilisation of the LUMO with increasing size is caused by cooperative interactions of the Ti 3d orbitals. The greatest changes are observed at the very smallest sizes (*e.g.* comparing monomer to dimer). More subtle changes in HOMO position are also observed across the series. Changes in coordination geometry at Ti, and surface structure, may also influence electronic structure across these size scales. Clusters with 7–18 Ti atoms appear to have similar energy gaps, with some showing minor red-shifts relative to $\mathbf{Ti_3}$, but all remain blue shifted relative to bulk TiO_2. To realise further notable changes in electronic structure the particles must become significantly bigger, *e.g.* approaching 100 Ti atoms.[18]

These results demonstrate that size effects in Ti/O systems are similar to other semiconducting oxides like ZnO, but that they occur only at very small (<2 nm) sizes at which point the structures have adapted from that of bulk TiO_2 and, therefore, other structural effects are also important. Understanding of these properties are crucial for the application of Ti/O based semiconducting materials constructed from ultrasmall Ti/O units, such as those found in Ti-based MOFs. The fundamental understanding of size effects at the smallest scales is also important for developing other metal oxide materials, enabling band gap engineering and frontier orbital positioning for photocatalyst materials and charge transport layers in electronic devices.

Author contributions

Concept by SDP, Synthesis and spectroscopy by TJB and SDP, Electrochemistry by ES, Computational studies by BW and FDP. All Authors contributed to preparing the manuscript.

Conflicts of interest

There are no conflicts to declare.

Data availability

All raw data has been deposited in the University of Warwick's database, WRAP, and can be found at **https://wrap.warwick.ac.uk/197288/**.

Supplementary information (SI): experimental methods, supporting characterisation and spectra, computational data, supporting notes. See DOI: https://doi.org/10.1039/d5qi02443a.

Acknowledgements

We are grateful for support from the Royal Society for a Royal Society University Research Fellowship supporting SDP and TJB (URF/R1/191458) and Research Grant (RG/R2/232264). TJB also acknowledges the University of Warwick CDT in Analytical Science. ES thanks the EPSRC for a studentship through a Doctoral Training Partnership (DTP) Grant. We thank the Macpherson Group at the University of Warwick for assistance with boron-doped diamond electrodes. BW and FDP acknowledge support of the Research Foundation Flanders (FWO) and the Vrije Universiteit Brussel through a Strategic Research Program awarded to the Research Group of General Chemistry (SRP73). We thank support from the EUTOPIA Connected Research Community scheme.

References

1 X. Chen, X. Peng, L. Jiang, X. Yuan, H. Yu, H. Wang, J. Zhang and Q. Xia, Recent advances in titanium metal–organic frameworks and their derived materials: Features, fabrication, and photocatalytic applications, *Chem. Eng. J.*, 2020, **395**, 125080.

2 Y. Sari, P. L. Gareso, B. Armynah and D. Tahir, A review of TiO2 photocatalyst for organic degradation and sustainable hydrogen energy production, *Int. J. Hydrogen Energy*, 2024, **55**, 984–996.

3 V. Kumaravel, K. M. Nair, S. Mathew, J. Bartlett, J. E. Kennedy, H. G. Manning, B. J. Whelan, N. S. Leyland and S. C. Pillai, Antimicrobial TiO2 nanocomposite coatings for surfaces, dental and orthopaedic implants, *Chem. Eng. J.*, 2021, **416**, 129071.

4 Y. Wei, Q. Wu, H. Meng, Y. Zhang and C. Cao, Recent advances in photocatalytic self-cleaning performances of TiO2-based building materials, *RSC Adv.*, 2023, **13**(30), 20584–20597.

5 M. A. Isaacs, C. Drivas, A. Graf, S. Kroon, S. Kumar, J. Liu, A. Torres-Lopez, C. Price, E. Garland, I. Lezcano-Gonzalez, C. M. A. Parlett, V. C. D. Santos-Durndell and L. J. Durndell, Understanding the Chemical and Electronic Properties of Sub-Monolayer TiO2 on High Surface Area Silica for Jet Fuel Synthesis Applications, *Adv. Funct. Mater.*, 2025, e02818.

6 Y. H. Lai, D. W. Palm and E. Reisner, Multifunctional Coatings from Scalable Single Source Precursor Chemistry in Tandem Photoelectrochemical Water Splitting, *Adv. Energy Mater.*, 2015, **5**(24), 1501668.

7 M. Mirsafaei, P. B. Jensen, M. Ahmadpour, H. Lakhotiya, J. L. Hansen, B. Julsgaard, H.-G. Rubahn, R. Lazzari, N. Witkowski, P. Balling and M. Madsen, Sputter-Deposited Titanium Oxide Layers as Efficient Electron Selective Contacts in Organic Photovoltaic Devices, *ACS Appl. Energy Mater.*, 2020, **3**(1), 253–259.

8 A. L. Efros and L. E. Brus, Nanocrystal Quantum Dots: From Discovery to Modern Development, *ACS Nano*, 2021, **15**(4), 6192–6210.

9 F. Pelayo García de Arquer, D. V. Talapin, V. I. Klimov, Y. Arakawa, M. Bayer and E. H. Sargent, Semiconductor quantum dots: Technological progress and future challenges, *Science*, 2021, **373**(6555), eaaz8541.

10 L. Manna, The Bright and Enlightening Science of Quantum Dots, *Nano Lett.*, 2023, **23**(21), 9673–9676.

11 V. Luca, Comparison of Size-Dependent Structural and Electronic Properties of Anatase and Rutile Nanoparticles, *J. Phys. Chem. C*, 2009, **113**(16), 6367–6380.

12 C. Maheu, L. Cardenas, E. Puzenat, P. Afanasiev and C. Geantet, UPS and UV spectroscopies combined to position the energy levels of TiO2 anatase and rutile nanopowders, *Phys. Chem. Chem. Phys.*, 2018, **20**(40), 25629–25637.

13 S. Monticone, R. Tufeu, A. V. Kanaev, E. Scolan and C. Sanchez, Quantum size effect in TiO2 nanoparticles: does it exist?, *Appl. Surf. Sci.*, 2000, **162–163**, 565–570.

14 N. Satoh, T. Nakashima, K. Kamikura and K. Yamamoto, Quantum size effect in TiO2 nanoparticles prepared by finely controlled metal assembly on dendrimer templates, *Nat. Nanotechnol.*, 2008, **3**, 106.

15 H. Peng and J. Li, Quantum Confinement and Electronic Properties of Rutile TiO2 Nanowires, *J. Phys. Chem. C*, 2008, **112**(51), 20241–20245.

16 A. V. Vorontsov and P. G. Smirniotis, Size and surface groups effects in decahedral anatase nanoparticles for photocatalytic applications, *J. Photochem. Photobiol., A*, 2018, **363**, 51–60.

17 P. Coppens, Y. Chen and E. Trzop, Crystallography and Properties of Polyoxotitanate Nanoclusters, *Chem. Rev.*, 2014, **114**(19), 9645–9661.

18 N. Serpone, D. Lawless and R. Khairutdinov, Size Effects on the Photophysical Properties of Colloidal Anatase TiO2 Particles: Size Quantization versus Direct Transitions in This Indirect Semiconductor?, *J. Phys. Chem.*, 1995, **99**(45), 16646–16654.

19 N. Sakai, Y. Ebina, K. Takada and T. Sasaki, Electronic Band Structure of Titania Semiconductor Nanosheets Revealed by Electrochemical and Photoelectrochemical Studies, *J. Am. Chem. Soc.*, 2004, **126**(18), 5851–5858.

20 H. O. Badr, T. El-Melegy, M. Carey, V. Natu, M. Q. Hassig, C. Johnson, Q. Qian, C. Y. Li, K. Kushnir, E. Colin-Ulloa, L. V. Titova, J. L. Martin, R. L. Grimm, R. Pai, V. Kalra, A. Karmakar, A. Ruffino, S. Masiuk, K. Liang, M. Naguib, O. Wilson, A. Magenau, K. Montazeri, Y. Zhu, H. Cheng, T. Torita, M. Koyanagi, A. Yanagimachi, T. Ouisse, M. Barbier, F. Wilhelm, A. Rogalev, J. Björk, P.OÅ. Persson, J. Rosen, Y.-J. Hu and M. W. Barsoum, Bottom-up, scalable synthesis of anatase nanofilament-based two-dimensional titanium carbo-oxide flakes, *Mater. Today*, 2022, **54**, 8–17.

21 T. J. Jacobsson and T. Edvinsson, Photoelectrochemical Determination of the Absolute Band Edge Positions as a Function of Particle Size for ZnO Quantum Dots, *J. Phys. Chem. C*, 2012, **116**(29), 15692–15701.
22 T. Edvinsson, Optical quantum confinement and photocatalytic properties in two-, one- and zero-dimensional nanostructures, *R. Soc. Open Sci.*, 2018, **5**(9), 180387.
23 J. Thyr, J. Montero, L. Österlund and T. Edvinsson, Energy Alignment of Quantum-Confined ZnO Particles with Copper Oxides for Heterojunctions with Improved Photocatalytic Performance, *ACS Nanosci. Au*, 2022, **2**(2), 128–139.
24 S. E. Brown and S. D. Pike, Photoabsorption of 1–2 nm molecular Ce-oxo nanoclusters versus ceria: intervalence charge transfer but no size effects, *Chem. Sci.*, 2025, **16**, 11659–11668.
25 J. Castillo-Lora, R. Mitsuhashi and J. M. Mayer, Revealing the Relative Electronic Landscape of Colloidal ZnO and TiO2 Nanoparticles via Equilibration Studies, *J. Phys. Chem. C*, 2019, **123**(16), 10262–10271.
26 W.-H. Fang, L. Zhang and J. Zhang, Synthetic strategies, diverse structures and tuneable properties of polyoxo-titanium clusters, *Chem. Soc. Rev.*, 2018, **47**, 404–421.
27 U. Schubert, Titanium-Oxo Clusters with Bi- and Tridentate Organic Ligands: Gradual Evolution of the Structures from Small to Big, *Chem. – Eur. J.*, 2021, **27**(44), 11239–11256.
28 U. Schubert and B. Stöger, Structural Chemistry of Titanium(IV) Oxo Clusters, Part 2: Clusters without Carboxylate or Phosphonate Ligands, *Chem. – Eur. J.*, 2024, **30**(31), e202400744.
29 T. Krämer, F. Tuna and S. D. Pike, Photo-redox reactivity of titanium-oxo clusters: mechanistic insight into a two-electron intramolecular process, and structural characterisation of mixed-valent Ti(iii)/Ti(iv) products, *Chem. Sci.*, 2019, **10**(28), 6886–6898.
30 S. E. Brown, I. Mantaloufa, R. T. Andrews, T. J. Barnes, M. R. Lees, F. De Proft, A. V. Cunha and S. D. Pike, Photoactivation of titanium-oxo cluster [Ti6O6(OR)6 (O2CtBu)6]: mechanism, photoactivated structures, and onward reactivity with O2 to a peroxide complex, *Chem. Sci.*, 2023, **14**, 675–683.
31 S. E. Brown, M. R. Warren, D. J. Kubicki, A. Fitzpatrick and S. D. Pike, Photoinitiated Single-Crystal to Single-Crystal Redox Transformations of Titanium-Oxo Clusters, *J. Am. Chem. Soc.*, 2024, **146**(25), 17325–17333.
32 A. Chikara, A. R. Veale, S. E. Brown, J. M. Woolley, F. De Proft and S. D. Pike, Switching on photoreactivity in Ti4-oxo clusters by increasing the size of 1,n-alkane diolate bridging ligands, *Chem. Sci.*, 2026, **17**, 1870–1879.
33 J. Castells-Gil, N. M. Padial, N. Almora-Barrios, I. da Silva, D. Mateo, J. Albero, H. García and C. Martí-Gastaldo, De novo synthesis of mesoporous photoactive titanium(IV)–organic frameworks with MIL-100 topology, *Chem. Sci.*, 2019, **10**(15), 4313–4321.
34 J. Wang, A. S. Cherevan, C. Hannecart, S. Naghdi, S. P. Nandan, T. Gupta and D. Eder, Ti-based MOFs: New insights on the impact of ligand composition and hole scavengers on stability, charge separation and photocatalytic hydrogen evolution, *Appl. Catal., B*, 2021, **283**, 119626.
35 C. T. Saouma, S. Richard, S. Smolders, M. F. Delley, R. Ameloot, F. Vermoortele, D. E. De Vos and J. M. Mayer, Bulk-to-Surface Proton-Coupled Electron Transfer Reactivity of the Metal–Organic Framework MIL-125, *J. Am. Chem. Soc.*, 2018, **140**(47), 16184–16189.
36 S. Wang, T. Kitao, N. Guillou, M. Wahiduzzaman, C. Martineau-Corcos, F. Nouar, A. Tissot, L. Binet, N. Ramsahye, S. Devautour-Vinot, S. Kitagawa, S. Seki, Y. Tsutsui, V. Briois, N. Steunou, G. Maurin, T. Uemura and C. Serre, A phase transformable ultrastable titanium-carboxylate framework for photoconduction, *Nat. Commun.*, 2018, **9**(1), 1660.
37 N. G. Altınçekiç, C. W. Lander, J. Yu, A. Roslend, Y. Shao and H. Noh, Proton, Electron, and Hydrogen-Atom Transfer Thermodynamics of the Metal–Organic Framework, Ti-MIL-125, Are Intrinsically Correlated to the Structural Disorder, *J. Am. Chem. Soc.*, 2025, **147**(38), 34777–34790.
38 T. J. Barnes, J. Payne and S. D. Pike, Synthesis of a nanoscale Cu(ii)31-oxo-carboxylate cluster, and effect of Cu–oxo cluster size on visible-light absorption, *Chem. Commun.*, 2023, **59**(1), 59–62.
39 M. Bochmann, G. Wilkinson, G. B. Young, M. B. Hursthouse and K. M. A. Malik, Preparation and properties of 1-adamantoxides, 2-adamantoxides, and 1-adamantylmethoxides of Ti, V, Nb, Nb, Cr, Cr, Mo, Mn, Fe, and Co. The crystal and molecular structure of tetrakis(1-adamantoxo)dimethylaminemolybdenum(IV), *J. Chem. Soc., Dalton Trans.*, 1980, (6), 901–910.
40 D. Stinghen, M. Atzori, C. M. Fernandes, R. R. Ribeiro, E. L. de Sá, D. F. Back, S. O. K. Giese, D. L. Hughes, G. G. Nunes, E. Morra, M. Chiesa, R. Sessoli and J. F. Soares, A Rare Example of Four-Coordinate Nonoxido Vanadium(IV) Alkoxide in the Solid State: Structure, Spectroscopy, and Magnetization Dynamics, *Inorg. Chem.*, 2018, **57**(18), 11393–11403.
41 A. Decken, G. B. Nikiforov and J. Passmore, The reaction of TiF4 with Li(OC(CF3)2Ph): direct synthetic route to the lithium–titanium heterometallic fluoride bridged complex {Li(THF)2TiF3(OC(CF3)2Ph)2}2 and Ti(OC(CF3)2Ph)4 alkoxide, *Dalton Trans.*, 2006, (36), 4328–4334.
42 T. J. Boyle, T. M. Alam, E. R. Mechenbier, B. L. Scott and J. W. Ziller, Titanium(IV) Neopentoxides. X-ray Structures of Ti3(μ3-O)(μ3-Cl)(μ-OCH2CMe3)3(OCH2CMe3)6 and [Ti(μ-OCH2CMe3)(OCH2CMe3)3]2, *Inorg. Chem.*, 1997, **36**(15), 3293–3300.
43 J. A. Ibers, Crystal and Molecular Structure of Titanium(IV) Ethoxide, *Nature*, 1963, **197**(4868), 686–687.
44 D. C. Bradley and C. E. Holloway, Nuclear magnetic resonance and cryoscopic studies on some alkoxides of titanium, zirconium, and hafnium, *J. Chem. Soc. A*, 1968, 1316–1319.
45 V. W. Day, T. A. Eberspacher, Y. Chen, J. Hao and W. G. Klemperer, Low-nuclearity titanium oxoalkoxides:

the trititanates [Ti3O](OPri)10 and [Ti3O](OPri)9(OMe), *Inorg. Chim. Acta*, 1995, **229**(1), 391–405.

46 V. W. Day, T. A. Eberspacher, W. G. Klemperer, C. W. Park and F. S. Rosenberg, Solution structure elucidation of early transition metal polyoxoalkoxides using oxygen-17 NMR spectroscopy, *J. Am. Chem. Soc.*, 1991, **113**(21), 8190–8192.

47 N. Steunou, F. Ribot, K. Boubekeur, J. Maquet and C. M. Sanchez, Ketones as an oxolation source for the synthesis of titanium-oxo-organoclusters, *New J. Chem.*, 1999, **23**(11), 1079–1086.

48 V. W. Day, T. A. Eberspacher, W. G. Klemperer and C. W. Park, Dodecatitanates: a new family of stable polyoxotitanates, *J. Am. Chem. Soc.*, 1993, **115**(18), 8469–8470.

49 N. Steunou, G. Kickelbick, K. Boubekeur and C. Sanchez, A new polyoxo-alkoxo titanium cluster of the Keggin family: synthesis and characterization by X-ray diffraction and NMR spectroscopy, *J. Chem. Soc., Dalton Trans.*, 1999, (21), 3653–3655.

50 R. Schmid, A. Mosset and J. Galy, New compounds in the chemistry of Group 4 transition-metal alkoxides. Part 4. Synthesis and molecular structures of two polymorphs of [Ti16O16(OEt)32] and refinement of the structure of [Ti7O4(OEt)20], *J. Chem. Soc., Dalton Trans.*, 1991, (8), 1999–2005.

51 C. F. Campana, Y. Chen, V. W. Day, W. G. Klemperer and R. A. Sparks, Polyoxotitanates join the Keggin family: synthesis, structure and reactivity of [Ti18O28H][OBut]17, *J. Chem. Soc., Dalton Trans.*, 1996, (5), 691–702.

52 W.-H. Fang, L. Zhang and J. Zhang, A 3.6 nm Ti52-Oxo Nanocluster with Precise Atomic Structure, *J. Am. Chem. Soc.*, 2016, **138**(24), 7480–7483.

53 Q.-Y. Zhu and J. Dai, Titanium oxo/alkoxyl clusters anchored with photoactive ligands, *Coord. Chem. Rev.*, 2021, **430**, 213664.

54 J.-X. Liu, M.-Y. Gao, W.-H. Fang, L. Zhang and J. Zhang, Bandgap Engineering of Titanium–Oxo Clusters: Labile Surface Sites Used for Ligand Substitution and Metal Incorporation, *Angew. Chem., Int. Ed.*, 2016, **55**(17), 5160–5165.

55 J. B. Benedict and P. Coppens, The Crystalline Nanocluster Phase as a Medium for Structural and Spectroscopic Studies of Light Absorption of Photosensitizer Dyes on Semiconductor Surfaces, *J. Am. Chem. Soc.*, 2010, **132**(9), 2938–2944.

56 P. R. Jubu, O. S. Obaseki, D. I. Ajayi, E. Danladi, K. M. Chahrour, A. Muhammad, S. Landi, T. Igbawua, H. F. Chahul and F. K. Yam, Considerations about the determination of optical bandgap from diffuse reflectance spectroscopy using the tauc plot, *J. Opt.*, 2024, **53**, 5054–5064.

57 Y.-Y. Wu, P. Wang, Y.-H. Wang, J.-B. Jiang, G.-Q. Bian, Q.-Y. Zhu and J. Dai, Metal–phenanthroline fused Ti17 clusters, a single molecular source for sensitized photoconductive films, *J. Mater. Chem. A*, 2013, **1**(34), 9862–9868.

58 P. Makuła, M. Pacia and W. Macyk, How To Correctly Determine the Band Gap Energy of Modified Semiconductor Photocatalysts Based on UV–Vis Spectra, *J. Phys. Chem. Lett.*, 2018, **9**(23), 6814–6817.

59 F. Babonneau, S. Doeuff, A. Leaustic, C. Sanchez, C. Cartier and M. Verdaguer, XANES and EXAFS study of titanium alkoxides, *Inorg. Chem.*, 1988, **27**(18), 3166–3172.

60 L. Marchese, E. Gianotti, V. Dellarocca, T. Maschmeyer, F. Rey, S. Coluccia and J. M. Thomas, Structure–functionality relationships of grafted Ti-MCM41 silicas. Spectroscopic and catalytic studies, *Phys. Chem. Chem. Phys.*, 1999, **1**(4), 585–592.

61 Y. Hu, G. Martra, J. Zhang, S. Higashimoto, S. Coluccia and M. Anpo, Characterization of the Local Structures of Ti-MCM-41 and Their Photocatalytic Reactivity for the Decomposition of NO into N2 and O2, *J. Phys. Chem. B*, 2006, **110**(4), 1680–1685.

62 S. Eslava, B. P. R. Goodwill, M. McPartlin and D. S. Wright, Extending the Family of Titanium Heterometallic–oxo–alkoxy Cages, *Inorg. Chem.*, 2011, **50**(12), 5655–5662.

63 J. V. Macpherson, A practical guide to using boron doped diamond in electrochemical research, *Phys. Chem. Chem. Phys.*, 2015, **17**(5), 2935–2949.

64 A. J. Bard, L. R. Faulkner and H. S. White, *Electrochemical methods: fundamentals and applications*, John Wiley & Sons, 2022.

65 V. Mansfeldova, M. Zlamalova, H. Tarabkova, P. Janda, M. Vorokhta, L. Piliai and L. Kavan, Work Function of TiO2 (Anatase, Rutile, and Brookite) Single Crystals: Effects of the Environment, *J. Phys. Chem. C*, 2021, **125**(3), 1902–1912.

66 C. Adamo and V. Barone, Toward reliable density functional methods without adjustable parameters: The PBE0 model, *J. Chem. Phys.*, 1999, **110**(13), 6158–6170.

67 V. N. Staroverov, G. E. Scuseria, J. Tao and J. P. Perdew, Comparative assessment of a new nonempirical density functional: Molecules and hydrogen-bonded complexes, *J. Chem. Phys.*, 2003, **119**(23), 12129–12137.

68 T. Yanai, D. P. Tew and N. C. Handy, A new hybrid exchange–correlation functional using the Coulomb-attenuating method (CAM-B3LYP), *Chem. Phys. Lett.*, 2004, **393**(1), 51–57.

69 J. P. Perdew, K. Burke and M. Ernzerhof, Generalized Gradient Approximation Made Simple, *Phys. Rev. Lett.*, 1996, **77**(18), 3865–3868.

70 F. Weigend and R. Ahlrichs, Balanced basis sets of split valence, triple zeta valence and quadruple zeta valence quality for H to Rn: Design and assessment of accuracy, *Phys. Chem. Chem. Phys.*, 2005, **7**(18), 3297–3305.

71 L. von Szentpály, P. Fuentealba, H. Preuss and H. Stoll, Pseudopotential calculations on Rb+2, Cs+2, RbH+, CsH+ and the mixed alkali dimer ions, *Chem. Phys. Lett.*, 1982, **93**(6), 555–559.

72 E. Berardo, H.-S. Hu, S. A. Shevlin, S. M. Woodley, K. Kowalski and M. A. Zwijnenburg, Modeling Excited

States in TiO_2 Nanoparticles: On the Accuracy of a TD-DFT Based Description, *J. Chem. Theory Comput.*, 2014, **10**(3), 1189–1199.

73 X. Zhang, C. Blackman, R. G. Palgrave, S. Ashraf, A. Dey, M. O. Blunt, X. Zhang, T. Liu, S. Sun, L. Zhu, J. Guan, Y. Lu, T. W. Keal, J. Buckeridge, C. R. A. Catlow and A. A. Sokol, Environment-Driven Variability in Absolute Band Edge Positions and Work Functions of Reduced Ceria, *J. Am. Chem. Soc.*, 2024, **146**(24), 16814–16829.

74 M. A. Zwijnenburg, The effect of particle size on the optical and electronic properties of magnesium oxide nanoparticles, *Phys. Chem. Chem. Phys.*, 2021, **23**(38), 21579–21590.